Soft Matter

Accepted Manuscript

ROYAL SOCIETY OF CHEMISTRY

www.rsc.org/softmatter

Coupling of gelation and glass transition in a biphasic colloidal mixture —from gel-to-defective gel-to-glass

Di Jia,[1,2] Javoris V. Hollingsworth,[1] Zhi Zhou,[1,2] He Cheng[3,4,*] and Charles C. Han[1,*]

[1]State Key Laboratory of Polymer Physics and Chemistry, Joint Laboratory of Polymer Science and Materials, Beijing National Laboratory for Molecular Sciences, Institute of Chemistry, Chinese Academy of Sciences, Beijing 100190, China

[2]University of Chinese Academy of Sciences, Beijing 100049, China

[3]China Spallation Neutron Source (CSNS), Institute of High Energy Physics (IHEP), Chinese Academy of Sciences (CAS), Dongguan 523803, China

[4]Dongguan Institute of Neutron Science (DINS), Dongguan 523808, China

[*] To whom correspondence should be addressed.

Phone: 86-010-82618089. Fax: 86-010-62521519. E-mail: chenghe@ihep.ac.cn; c.c.han@iccas.ac.cn

Abstract

The state transition from gel to glass is studied in a biphasic mixture of polystyrene core/poly (*N*-isopropylacrylamide) shell (CS) microgels and sulfonated polystyrene (PSS) particles. At 35 ℃, the interaction between CS microgels is due to short-range Van der Waals attraction, while that between PSS particles is from long-range electrostatic repulsion. During variation of the relative ratio of the two species at a fixed apparent total volume fraction, the mixture exhibits a gel-to-defective gel-to-glass transition. When small amounts of PSS are introduced into the CS gel network, some of them are kinetically trapped, causing a change in its fractal structure, and act as defects to weaken the macroscopic gel strength. An increase of PSS content in the mixture promotes the switch from gel to defective gel, *e.g.*, the typical two-step yielding gel merges into one-step yielding. This phenomenon is an indication that inter-cluster bond breakage coincides with intra-cluster bond fracture. As the relative volume fraction of PSS exceeds a critical threshold, the gel network can no longer be formed; hence, the mixture exhibits characteristics of glass. A state diagram of the biphasic mixture is constructed, and the landscape of the different transitions will be described in future studies.

1 Introduction

The non-equilibrium states of gel and glass in colloidal suspensions are of great importance from both technological and academic points of view.[1-3] For instance, gel and glass forming colloidal systems provide a variety of useful properties for

industrial products, such as food,[4] cosmetics,[5] coatings and processing.[6] Such colloids can also act as "big atoms" and its equilibrium or non-equilibrium state transitions have been used to model phase transitions of molecular systems in condensed matter physics.[7, 8] This particular concept has been demonstrated in the study of yielding behaviors of repulsive glass and gel. For typical one-component repulsive glass, the observed one-step yielding is generally attributed to the breaking of local topological constraints.[9-11] For binary hard sphere glass with relatively large size disparities, two-step yielding happens due to the two different length scales of small and large sphere cages[12] and the composition of the mixture determines the caging mechanism[13]. However, when two length-scale particles exist in a soft glass, the cage of a large particle is determined by both the large and small particles around it.[14] In contrast, gels usually exhibit two-step yielding, where the first step corresponds to the weakest bond breakage of inter-clusters, while the second is due to fragmentation of clusters and breaking of intra-cluster bonds.[15-18] Therefore, two-step yielding behavior reflects structural heterogeneities which often occur in systems with two different competing length or time scales.[19]

In previous studies, the investigated models were limited to pseudo one-component systems. The coupling of gelation and glass transition has received less attention, mainly because of the difficulty of finding a model colloidal system where thermal fluctuation still plays an influential role in the transition process. For such an objective, biphasic colloid mixtures are well-suited.[20, 21] A typical biphasic system is composed of two species with equal size, one of which interacts via short-range

attraction and another experiences long-range repulsion. In comparison to traditional one-component systems, whose structure is only tuned by the combination of inter-particle interaction, U, total volume fraction, Φ, and applied stress, σ,[22] the structure and strength of biphasic mixtures can be precisely controlled by the ratio of the two species at fixed total volume fraction Φ and interaction potential U. This approach combines the desirable properties of glass and gels, which include high solids loading and the resistance to consolidation, respectively.[23] Mohraz *et al.*[24] studied the dynamics of biphasic mixtures composed of partially hydrophobic and hydrophilic colloids. In their report, the two species are found to influence each other, *e.g.*, repulsive particles make attractive particles form more spatially homogeneous structures which share less bonds with other attractive species, while attractive species make repulsive particles exhibit dynamical heterogeneity. However, the structure evolution of biphasic mixtures during the coupling of gelation with glass transition still remains open for consideration.

In this study, a new biphasic system is designed to understand the state transition from gel to glass. Polystyrene core/poly (*N*-isopropylacrylamide) shell (CS) microgels are used as attractive species. When the temperature surpasses the volume phase transition temperature (VPTT) of them, an attraction between the species occurs due to the release of bond water.[25] For the repulsive species, sulfonated polystyrene (PSS) particles are chosen (the weak attraction between CS and PSS above VPTT is ignored). The relative fraction of CS/PSS in a biphasic mixture is changed at a fixed intermediate apparent total volume fraction Φ_{total}. When a small amount of PSS

particles are mixed with attractive microgels, the attractive species form a gel network while some of the PSS particles are dispersed within the gel domains, acting as defects to weaken the gel strength. When the relative fraction of the PSS species is gradually increased, the gel structure and its fractal dimension change correspondingly. When the relative fraction of PSS is above a critical point the gel network cannot be formed and the system jams into a glassy state, causing a gel-glass transition to occur. Lastly, a state diagram of the biphasic system is proposed. The structure evolution of gel-to-defective gel-to-glass provides insight for understanding the heterogeneity in the gel network, as well as the different mechanisms of gels and glass. These findings may lead to potential applications in many fields, such as biphasic inks of direct-write assembly[26-28] and biological field.[29]

2. Experimental section

2.1 Materials

Styrene (St, 98%, Sinopharm Chemical) was purified by passing through a basic alumina column to remove the inhibitor, *N*-Isopropylacrylamide (NIPAM, 97%, Aldrich) was purified by recrystallization in hexane, sodium dodecyl sulphate (SDS, 99%, Beijing Chemical), potassium peroxodisulfate (KPS, ≥99%, Sigma-Aldrich), *N,N'*-methylenebisacrylamide (BIS, 99%, Alfa Aesar), potassium chloride (KCl, 99%, Amethyst Chemicals), and concentrated sulfuric acid (95-98%, Beijing Chemical), ethanol (95%, Beijing Chemical) were used as received. Water was obtained from a Milli-Q water purification system (Millipore, Bedford, MA, USA). 0.2 μm fluorescent

sulfate microspheres (F-8848) was purchased from Invitrogen Company. The sub-micrometer polystyrene particles were kindly provided by BASF Company. Coverslips (Catalog No.12-548-B) were purchased from Fisher Scientific Company.

2.2 Synthesis of Core Latex

The synthesis of polystyrene core and poly (*N*-isopropylacrylamide) shell particles followed the procedure of Ballauff *et al.*[30] 2.40 g SDS, 13.52 g NIPAM were dissolved in 1000 mL pure water in a reaction flask with a magnetic stirrer. Argon was bubbled through the mixture for 15 min. Next, 256.50 g styrene was added and the mixture was heated to 80 ℃. Argon was bubbled through the reaction mixture for another 30 min. 0.60 g KPS dissolved in 30 mL of water was added through a syringe. The reaction was allowed to continue at 80 ℃ for 8 hrs with a stirring speed of 400 rpm. The resulting suspension was extensively dialyzed against pure water until its conductivity was less than 1 mS/cm[31] for purification after removing the coagulum.

2.3 Synthesis of Core-Shell Microgels

129.10 g core latex (solids content 21.4 wt%) was diluted with 1000 mL of water, then 34.20 g NIPAM and 2.32 g BIS (the cross-linking degree is 5 mol%) were added. The reaction mixture was heated to 80 ℃ under argon atmosphere. 0.72 g KPS dissolved in 30 mL of water was quickly added to start the reaction while the mixture was stirred at 400 rpm for 5 hrs. The product was centrifuged and washed by water several times. Finally, the sample was lyophilized to form powders.

2.4 Synthesis of Sulfonated Polystyrene (PSS) Particles

22.60 g of freeze-dried polystyrene particles were slowly immersed in a large amount of concentrated sulfuric acid (98%, 246 mL), then the sample was homogenized by ultrasonic waves for 15 min. Next, the sample was stirred at 40 ℃ for 1 hr. Finally, the product was centrifuged and washed first by ethanol and then by water several times until the pH of the particle suspension was about 5. Upon completion, the particles were freeze-dried before use.

2.5 Preparation of Biphasic Mixture

CS and PSS particles were mixed in 0.05M KCl solutions at fixed apparent total volume fraction Φ_{total} =32% for all the rheological experiment. The mixed suspension was then homogenized by ultrasonic waves at room temperature for 20 min. The lid of the vial was sealed with parafilm to avoid water evaporation. To fully swell the CS particles, the samples were placed in a refrigerator for 2 days. The confocal sample cell was an aluminous dish (ϕ =35 mm) with a hole (ϕ =14 mm, height of 0.1~0.15 mm) in the bottom center. The glass cover slip was fixed onto the bottom hole with glue. The sample was then exposed to ultrasound for 15 min before use, then 6 μL (Φ_{total} =10% was fixed for all the confocal microscopy experiment) was added into the sample cell. Another glass cover slip was put on the upper surface of the hole and sealed with silicone oil to form a three-dimensional sealed space. The prepared

sample cell was mounted onto the table of a confocal laser scanning microscope for observation.

2.6. Instrumentation

Rheological measurements were performed with a stress-controlled rheometer (Anton Paar MCR 502), using a 25 mm roughened cone–plate geometry. Silicone oil was coated on the edge of the cone-plate to prevent water evaporation. All yielding measurements were carried out in strain control mode with fixed frequency (ω =10 rad/s) and strain amplitude at 35 ℃.

A spinning-disk high resolution confocal microscope (Andor Revolution) equipped with a 100× oil objective (Olympus NA =1.4) was used. Confocal images were collected through an emission filter (685 ± 20 nm), captured by an EMCCD (Andor iXon 897) with 100 ms exposure time and 100×EM gain. Another confocal microscope (FV1000-IX81, Olympus, Japan) equipped with a 100× oil objective (Olympus NA =1.4) was also used. A laser with a wavelength of 488 nm was used to excite the fluorescent particles (E_x/E_m: 505/515). Bright-field and fluorescent images could be collected simultaneously and then merged into one image.

Dynamic light scattering was performed on a modified laser light scattering spectrometer (ALV/DLS/SLS-5022F) equipped with a multi-τ digital time correlator (ALV5000) and four lasers with different wavelengthes.[32] A cylindrical 22 mW UNIPHASE He−Ne laser (λ_0 = 632.8 nm) was used to do the test. The scattering angle is 30 °. The baseline-normalized intensity−intensity time correlation function $g^{(2)}(t)$ in

the self-beating mode was measured. The CONTIN program was used to calculate the hydrodynamic radius distribution.

3. Results

3.1 Characterization of Biphasic Mixture

To screen the electrostatic interaction due to residual charges affixed to the PS core in CS microgel, 0.05M KCl was added to the suspensions.[33] The Debye length of CS microgel is 1.4 nm, which is much smaller than the shell thickness, and the electrostatic interaction between CS microgels is negligible. Therefore, the CS suspension at Φ_{total} =32% becomes a gel due to Van der Waals attraction when the temperature is higher than the VPTT (volume phase transition temperature). Also the Zeta potential of PSS particles suspended in 0.05M KCl solution is -45 mV; due to electrostatic repulsion, PSS particles are still stable in 0.05M KCl solution at 35 ℃.

The hydrodynamic radius R_h of the CS microgels as a function of temperature is shown in Fig. 1. As temperature increases from 16 ℃ to 50 ℃, R_h decreases from 191 nm to 128 nm. Above the VPTT (32 ℃), the microgel remains stable as a result of electrostatic repulsion without salt, but flocculates with salt. At 35 ℃, R_h is 127 nm and the z-averaged half-width at half maximum (HWHM) is 29 nm corresponding to a relative standard deviation of the particles size distribution (PSD)[34] σ =0.2, indicating the CS microgels are monodispersed. PSS particles have an R_h of 130 nm and HWHM is 41 nm (σ =0.3), nearly the same as that of CS particles at 35 ℃, which facilitates the modeling of the biphasic mixture[20]. The inset shown in Fig. 1 is the R_h

distribution of both CS microgels and PSS particles at 35 ℃. It should be noted that the size of the particles should be small enough to enable thermal fluctuation to influence its thermodynamics.

The effective volume fraction of charged PSS particles should be calculated by the effective interaction radius R_{HS} which considers the long-range electrostatic interaction. R_{HS} is larger than the actual particle radius,[35] which depends on the ionic strength and particle concentration. Since the interaction potential depends on concentration, it is difficult to determine the effective volume fraction of PSS at each concentration precisely, especially at such high concentration regime. Therefore, weight fraction is directly converted to volume fraction Φ_{PSS} using a density of 1.05 (g/cm^3) for PS. The volume fraction of CS particles Φ_{CS} is determined by[33]

$$\Phi_{CS} = \Phi_C \left(\frac{R_h}{R_C}\right)^3 \quad (1)$$

Where Φ_C is the volume fraction of core particles, R_C is the core radius (R_C =73 nm determined by DLS) and R_h is the hydrodynamic radius of CS microgels. The apparent total volume fraction of biphasic mixtures is $\Phi_{total} = \Phi_{PSS} + \Phi_{CS}$. For all the rheological experiments, Φ_{total} =32% is fixed and the symbol "CS84" indicates Φ_{CS}/Φ_{total} =84%.

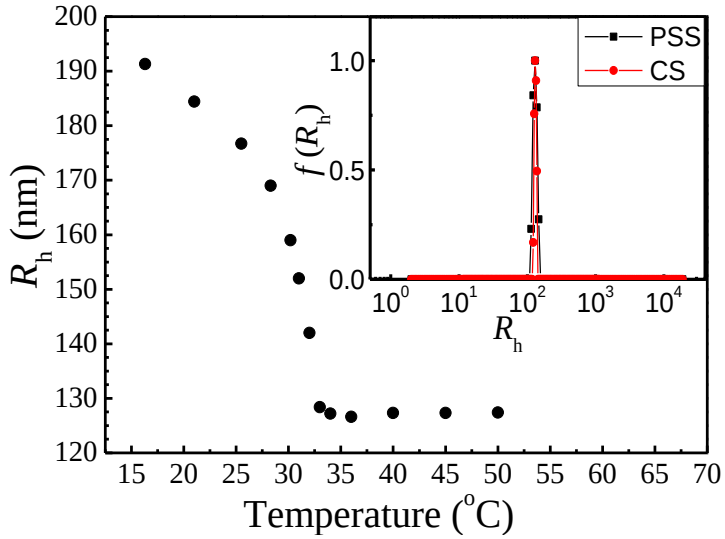

Fig. 1 Temperature dependence of hydrodynamic radius R_h of CS particles. Inset is the R_h distribution of both PSS particles and CS microgels at 35 ℃.

3.2 Dynamic Frequency Sweep Investigation

Fig. 2 shows dynamic frequency sweep at different relative volume fraction of CS at fixed Φ_{total} =32% at 35 ℃. For all the samples, γ =1% is in the linear viscoelastic regime. As Φ_{PSS} increases, the storage modulus G' first decreases when Φ_{PSS}/Φ_{total} is lower than 16%, then increases with the further increase of Φ_{PSS}. The observed decrease of G' probably originates from the kinetic trapping of repulsive PSS particles in the percolation network during the gelation process. For another biphasic system, Mohraz *et al.*[24] reported that during the attractive species aggregating process, some repulsive particles would be kinetically trapped in the gel network, causing attractive particles to share fewer bonds with their neighbors. These trapped PSS particles act as defects in the gel network, and their presence may not only makes attractive particles share fewer bonds, but also weakens the average bond strength. It should be noted that the real volume fraction of PSS is larger than Φ_{PSS} converted from weight fraction

using a density of 1.05 (g/cm^3). In general, this occurrence is a result of long-range electrostatic repulsion.[35] Hence, with the increase of Φ_{PSS}/Φ_{total}, the real total volume fraction increases (apparent total volume fraction $\Phi_{total}=\Phi_{PSS}+\Phi_{CS}$ is fixed). Although the real total volume fraction of unary gel (CS100) is smaller than that of defective gels (CS84, CS75), its modulus is still larger.

The introduction of PSS defects also changes the fractal dimension of the biphasic mixture. The fractal dimension applied in the colloidal mixture with intermediate volume fraction can provide a qualitatively comparison of structure variation[18, 36]. For CS100, CS84 and CS75, G' fits a power law relation of $G' \sim \omega^n$ over more than two decades of frequency, which is a characteristic of gels.[37-39] The power law exponent n is related to the fractal dimension d_f, which describes the spatial distribution of mass within a network, according to the following expression:[40-42]

$$n = \frac{d(d+2-2d_f)}{2(d+2-d_f)} \quad (2)$$

where d is space dimension (d =3). Gradually, d_f increases weakly from 2.35 to 2.41 as CS content decreases from CS100 to CS75. The increase of fractal dimension reflects the gradual change of the gel structure. When Φ_{PSS} is above a critical threshold, the gel network can no longer be formed. The biphasic mixture then goes into a glassy state (CS60, CS50). The elastic modulus of glass is larger than that of gel and is almost independent of frequency, which suggests the jammed glass structure is stronger and more stable.

The frequency dependence of loss modulus G'' also proves the occurrence of gel-to-defective gel-to-glass transition. After the formation of the gel, G'' shows a minimum at frequencies much lower than that of glass, indicating a long-time α relaxation inside the gel phase.[39] However, for glass the minimum of G'' is related to the in-cage to out-of-cage transition or the characteristic time for a particle to explore its cage.[10] Therefore, based on the dynamic frequency sweeps at fixed Φ_{total}, there is a Φ_{PSS} dependence of gel-to-defective gel-to-glass transition, which can be reaffirmed by yielding experiments.

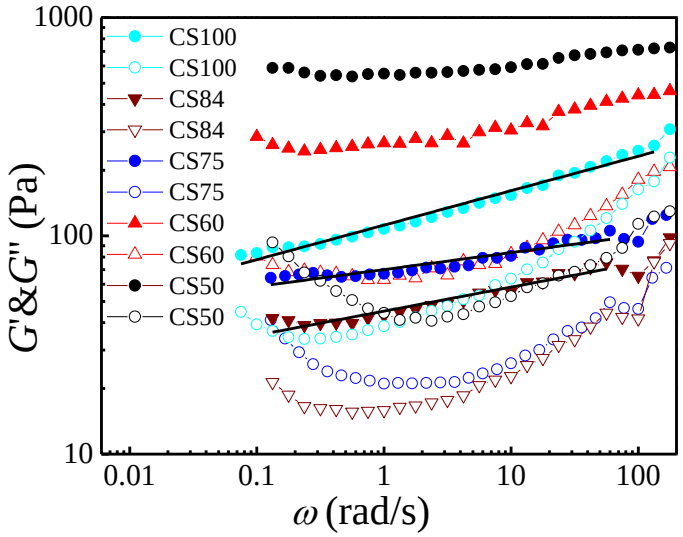

Fig. 2 Dynamic frequency sweeps at 35 ℃, γ=1% , Φ_{total} =32% is fixed and Φ_{CS} /Φ_{total} is 100%, 84%, 75%, 60%, 50% , respectively. Closed (open) symbols represent storage (loss) moduli. Black lines indicate the best fit.

3.3 Yielding Behavior Study

3.3.1 Gel-to-Defective Gel Transition

Fig. 3a and 3b are the total stress σ and elastic stress $\gamma G'$ as a function of strain for CS100, CS94, CS84, CS75; They show similar trend. The yield point is the location

where the curve becomes sub-linear or exhibits a peak. A typical gel (CS100) has two-step yielding, *e.g.*, the first (γ_1) corresponds to the bond breakage of inter-clusters and the second (γ_2) is the further breaking of intra-cluster bonds and fragmentation of dense clusters.[15-17] The addition of PSS particles weakens the gel network and makes the gel structure more homogeneous. This phenomenon is due to kinetically trapped PSS particles existing in the network during the gelation process, which allows the particles to act as defects to weaken and loosen gel bonds, making the bonds more flexible. Therefore, the first yield strain γ_1 moves to a higher strain as Φ_{PSS} increases. After the first yielding occurs, the gel network ruptures into disconnected clusters, but the system still cannot flow since G' is still larger than G'' after the first yielding (Fig. 4). It should be noted that with increasing Φ_{PSS}, more weakest bonds (located where PSS defects exist) break up during the first yielding, consequently smaller disconnected clusters will come up. The cluster length scale, which characterizes the structural heterogeneities,[16] decreases as Φ_{PSS} increases. Thus, the second yield strain γ_2 shifts to a lower strain and becomes broader and less pronounced probably due to the smaller cluster size. Finally, for CS75, the inter-cluster and intra-cluster bond breakage tend to superimpose, so the two-step yielding merges into one-step yielding. This is a clear indication of the biphasic mixture going from a typical gel into defective gel region.

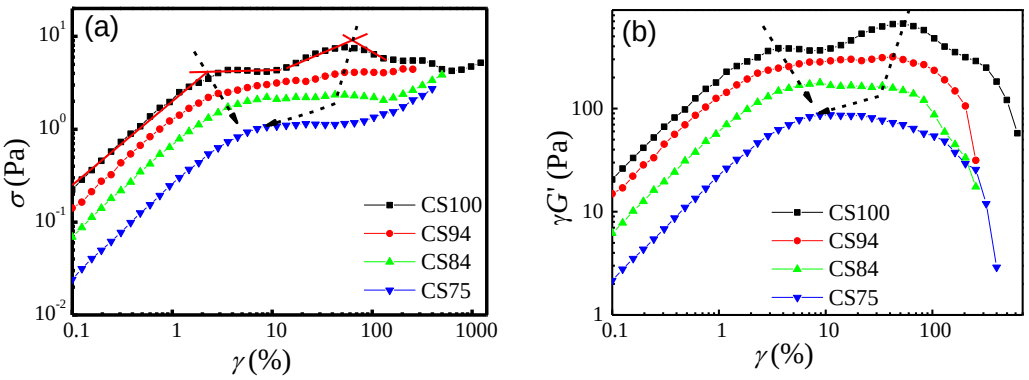

Fig. 3 (a) Total Stress σ during a dynamic strain sweep of sample CS100, CS94, CS84, and CS75 with fixed Φ_{total} =32% at ω =10 rad/s. (b) Elastic stress, $\gamma G'$ for the same data. The data of CS94 and CS75 are shift by 1.5× and 0.25× in both (a) and (b). The arrows are used to guide the eye to indicate the first and second yielding points.

An alternative representation of yielding behavior involves the strain dependence of storage and loss moduli (Fig. 4). After the first yielding, although cluster release could make G' and G'' decrease heavily, G' is still larger than G''. This is perhaps due to the residual elasticity of the remaining clusters, as well as the possibility of dynamically reforming bonds.[16] Generally, when the shear rate (frequency) approaching zero, the elasticity of the remaining clusters cannot be detected anymore, but bonds can totally reform , so the zero-shear rate liquid would not be observed. PSS particles act as defects and decrease the chance of bond reforming between attractive species and the size of disconnected clusters decreases as Φ_{PSS} increases. Therefore, the crossover point γ_C of G' and G'' shifts to lower strain as Φ_{PSS} increases.

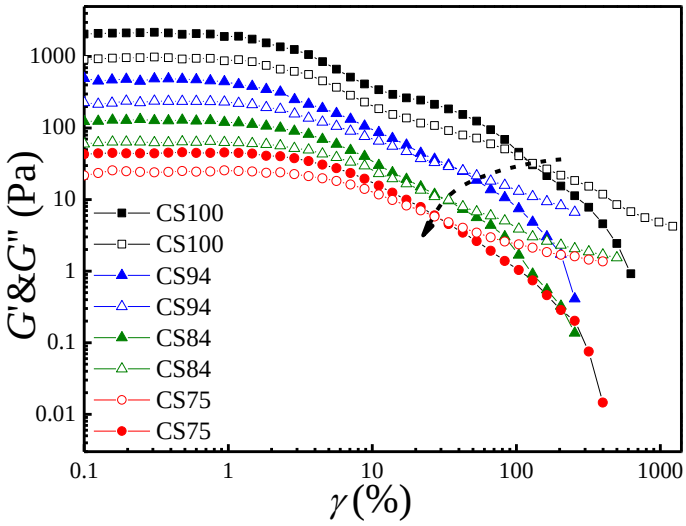

Fig. 4 Dynamic strain sweeps of sample CS100, CS94, CS84, and CS75 with fixed Φ_{total} =32% at ω=10 rad/s. The closed symbols represent storage modulus (G') and open symbols represent loss modulus (G''). The data are shifted by 0.5×, 2×, 5×, 10× from bottom to top. The arrow is used to guide the eye to indicate the crossover points γ_C of G' and G''.

3.3.2 Defective Gel-to-Glass Transition

The total stress σ and elastic stress $\gamma G'$ dependence of strain are monitored for CS75, CS72, CS70, CS68, CS60 and CS50 in Fig. 5. Both plots show similar trend. When Φ_{PSS}/Φ_{total} is lower than 40%, the biphasic mixtures are defective gels. The presence of PSS defects makes the gel network more homogeneous, which is indicated when inter-cluster breakage and intra-cluster disassembly merge into one broad yielding peak at 7%.

When Φ_{PSS} is higher than a critical threshold (CS60 and CS50), gel network can no longer be formed and the biphasic mixture becomes a glass. The yielding strain of glass jumps to ~20%, indicating the breakage of topological cages. Further increase of

Φ_{PSS} leads to a larger real total volume fraction and smaller cage sizes, resulting in a decrease in yielding strain. Figure 5 also shows that the yielding process of defective gels is much more gradual than that of glass. Typically, the yielding behavior of soft microgels (CS) is predominantly by long-range structural relaxations, while that of hard spheres (PSS) is short-ranged. Therefore, soft microgels have a more gradual yielding behavior than that of hard spheres.[43] So as Φ_{PSS} increases, the mixture jams into a glassy state with a yielding behavior which becomes relatively short-ranged and abrupt.

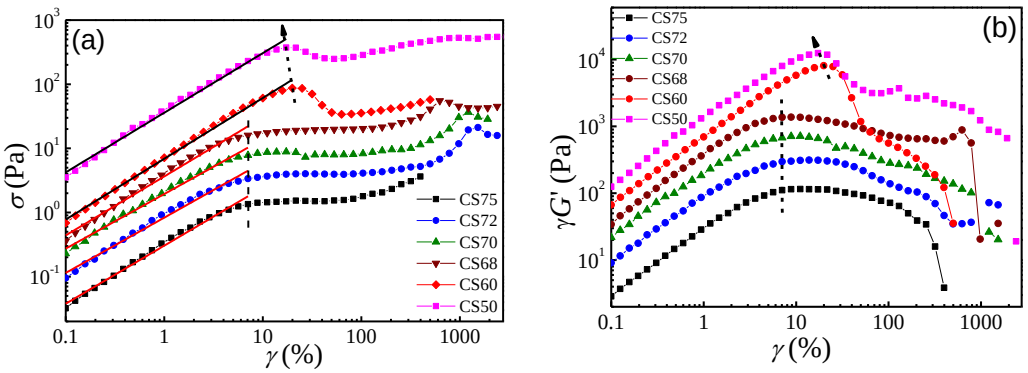

Fig. 5 (a) Total Stress σ during a dynamic strain sweep of CS75, CS72, CS68, CS60, and CS50 with fixed Φ_{total} =32% at ω =10 rad/s. (b) Elastic stress $\gamma G'$ for the same data. The data are shifted by 3/, 2/, 1×, 1.4×, 1.6×, 2×from bottom to top in both (a) and (b). The dashed lines are used to guide the eye to indicate the yielding points.

The defective gel-to-glass transition is better seen from the strain dependence of modulus in Fig. 6. In the defective gel region (from CS75 to CS68), the plateau elastic modulus increases with decreasing Φ_{CS}/Φ_{total}, as shown in the inset of Fig. 6. Schweizer *et al.*[20] predicted in theory that the elastic modulus of an ideal biphasic

mixture decreases as the relative fraction of attractive species increases when the attraction is weak (< $2k_BT$). Wu *et al.*[44] reported that the inter-particle potential between PNIPAM microgels at 35 ℃ is about $1k_BT$, which is just within the weak attraction range. Therefore, our results are consistent with the theoretical prediction of Schweizer. In addition, the real total volume fraction increases with Φ_{PSS}, which also contributes to the increase of elastic modulus. In the defective gel regime (from CS75 to CS68), γ_C becomes smaller and moves closer to the yielding point as Φ_{PSS} increases. This occurrence is perhaps due to the relatively lower probability of bonds reforming between attractive species after yielding when more PSS particles are trapped in the gel network. When the PSS content is higher than a critical threshold (CS60 and CS50), the mixture directly jams into a glassy state. The yielding behaviors of CS60 and CS50 show typical characteristics of glass, which has a viscous modulus G'' that exhibits a prominent maximum at the crossover point of G' and G''[11], as shown in Fig. 6.

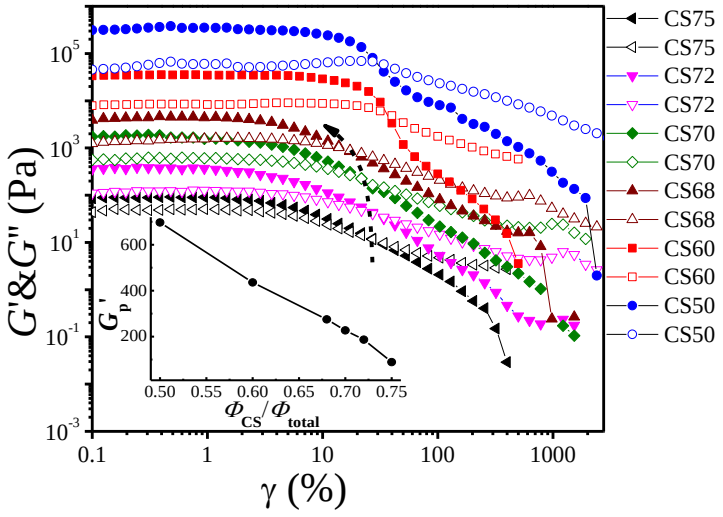

Fig. 6 Dynamic strain sweeps of samples with different PSS content (Φ_{total} =0.32) at ω=10 rad/s. The closed symbols represent storage modulus (G') and open symbols

represent loss modulus (G''). The data are shifted by 1×,2×,8×,16×,80×, and 500× from bottom to top. The arrow is used to guide the eye to indicate the crossover points γ_C of G' and G''. The inset summarizes the plateau elastic modulus G_p' against Φ_{CS}/Φ_{total} in the linear viscoelastic regime.

3.4 Confocal Microscopy of Biphasic Mixtures

To confirm and visualize the architecture of the binary gel clearly, high resolution confocal microscopy was used to directly observe the morphology of CS84 (Φ_{CS}/Φ_{total}=84%) with Φ_{total} =0.1. Because polystyrene particle is opaque to light, images of more concentrated sample cannot be obtained. A small amount of 0.2 μm fluorescent PSS particles (1/3000) were used as tracer particles to mix with non-fluorescent PSS species. The sample was maintained for 15 min at 35 ℃ until the gel structure was formed. As shown in Fig. 7, the CS microgels form a percolated network and the red fluorescent PSS particles display a heterogeneous distribution, *e.g.*, some of them are trapped inside the gel network, while others are in the voids or on the periphery. Mohraz *et al.*[24] studied the dynamics of another biphasic mixture and they proposed that repulsive species exhibit dynamical heterogeneity, some of them are trapped inside gel clusters during the aggregation process while others can freely move. The trapped repulsive PSS particles make attractive CS species share less bonds with others, thus form more spatially homogeneous structure. It reaffirms the assumption of defective gels, which is also in agreement with the previous rheological results. Small biphasic particles with radiuses of ~100 nm are used as

model system where thermal fluctuation still plays an influential role. Meanwhile, we are still working on time-resolved quantitative OM measurements in a biphasic micron-size-particle system.

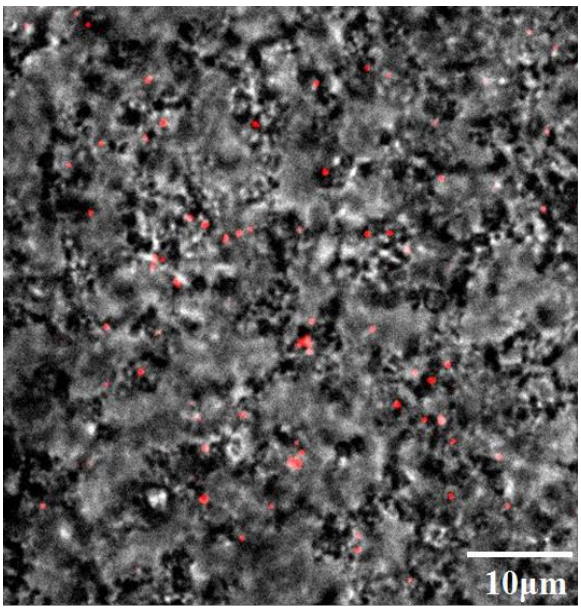

Fig. 7 High resolution confocal image of binary gel CS84 (Φ_{total} =0.1) at 35 ℃. Observation region is 51.2 μm×51.2 μm.

In order to further study the gradual change of the morphology of the biphasic mixtures at different Φ_{CS}/Φ_{total} (Φ_{total}= 0.1 is fixed), a series of confocal images were taken from CS100 to CS50. The ratio of fluorescent PSS tracer particles and non-fluorescent PSS species is Φ_{tracer}: Φ_{total}= 1:25000. The gel formation process is shown in the supporting information and the final morphology exhibits in Fig. 8. From CS100 to CS75, the gel network becomes less coarsening and the clusters which comprise gel network become smaller with Φ_{PSS} increasing. Finally, for CS60 and CS50, no gel network can form, only clusters can be observed. As we know, two-step yielding often occurs in systems with two competing length scales and/or time scales

interactively.[12, 15, 18, 19, 45, 46] When the quiescent structures in Figure 8 are under shear, two-step yielding probably happens because the gel network and cluster may be two length-scales during yielding. With the increase of Φ_{PSS}, defects are increasing in number, thereby decreasing the size of cluster. So the inter-cluster and intra-cluster bond breakages probably occur at the same time during the yielding process, and two-step yielding merges into a broad one-step yielding. With the further increase of Φ_{PSS}, no gel network can be formed anymore and only clusters and PSS particles coexist in CS60 and CS50.

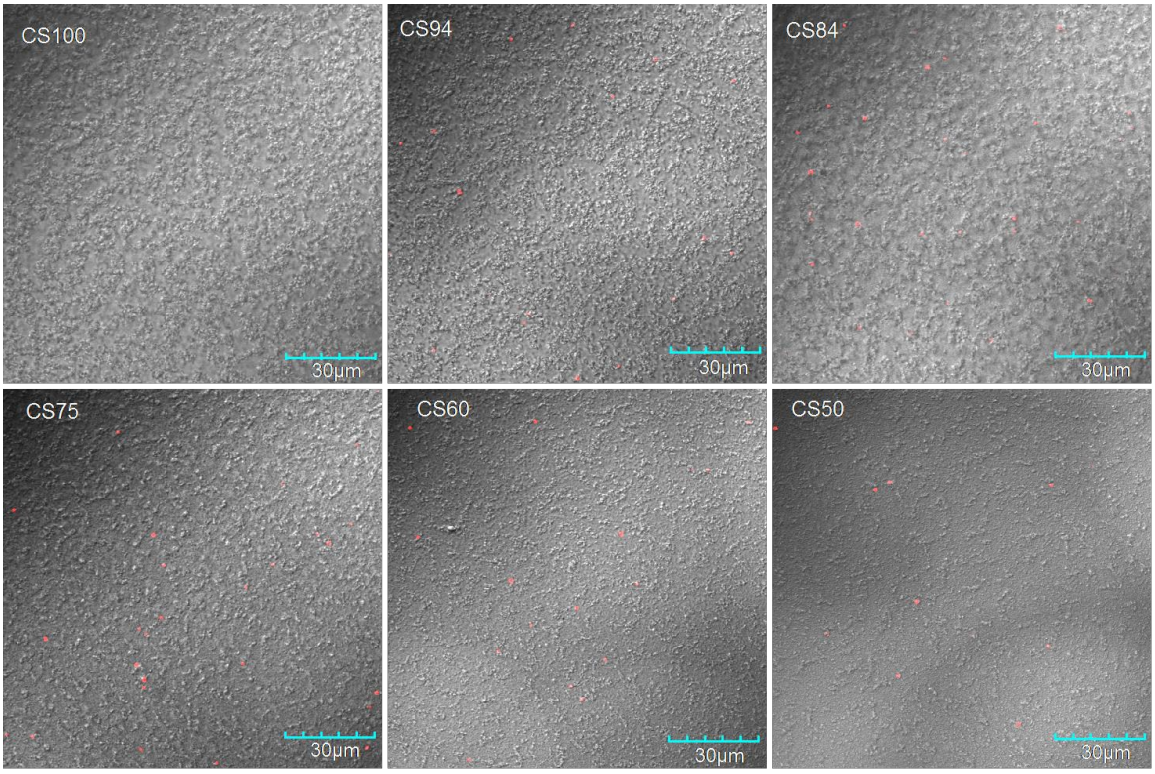

Fig. 8 Confocal images of sample CS100, CS94, CS84, CS75, CS60 and CS50, respectively with fixed Φ_{total} =0.1 at 35 ℃.

4. Discussion

4.1 Summary of Yield Strain $\gamma_1, \gamma_2, \gamma_C$ and elastic modulus at Different States

In Fig. 9, the yield strains are summarized as a function of CS relative fraction Φ_{CS}/Φ_{total} with fixed Φ_{total} =0.32. Fig. 9a can be divided into three regimes, *e.g.*, gel, defective gel and glass, respectively. Gel (black rectangular region) displays two-step yielding, where the first yield strain γ_1 indicates inter-cluster bond breakage and increases slightly with Φ_{PSS} from 2% to 4%. While the second yield strain γ_2 is attributed to intra-cluster bond breakage and fragmentation of clusters into smaller constituents. When Φ_{CS} further decreases, the system goes into a defective gel regime (blue rectangular region), only exhibiting one-step yielding which suggests a combination of inter-cluster and intra-cluster bond breakage. Also, the yield strain remains constant at 7%. When Φ_{CS} is below a threshold, biphasic particles jam with each other to form a glass. In the glass regime (red circular region), one-step yielding is still observed at ~20%, signifying the breakage of topological cages. In addition, as Φ_{PSS} further increases, the yield strain decreases due to the decrease of free volume. Fig. 9b shows the crossover yield strain, γ_C of G' and G'' as a function of Φ_{CS}/Φ_{total}. In both gel and defective gel regions, γ_C decreases with increasing Φ_{PSS} because the probability of bonds reforming after yielding gets lower and the residual elasticity of the remaining clusters decreases as more PSS particles are trapped inside the gel. In the glass region, the crossover yield strain γ_C appears at the maximum of loss modulus G'' (Fig. 6), which indicates that the breakup of topological cages leads to the system flowing. Note that γ_C of unary gel, CS100, is much larger than that of binary gel, which can be attributed to better elasticity of disconnected clusters and/or a higher probability of bonds reforming after the first yielding. The addition of only 6% PSS

particles (CS94) makes γ_C drop dramatically from 130% (CS100) to 43%. This unique property of a biphasic mixture makes it a great candidate for microfluidic and direct-write assembly techniques, where the sample must readily flow when it yields, *e.g.* passing through microchannels or fine deposition nozzles.[23, 27]

The elastic modulus of gel is dominated by bond effect while that of glass is dominated by cage effect. Generally, bond strength is much larger. While PSS particles are charged particles, their cage effect also contributes significantly due to long-range electrostatic repulsion. So there is a competition between bond and cage effect. CS100 is a unary gel whose elastic modulus is dominated by bonding. With the increase of PSS defects, bond effect decreases and cage cannot be formed when PSS concentration is not high enough, so the modulus decreases first. As Φ_{PSS} increases further, cage effect begins to contribute to the modulus (real total volume fraction increases) and bond effect contributes less (gel bonds are weakened by PSS defects). So in the defective gel region, the modulus of CS75 is larger than that of CS84 (Fig. 2). Finally, the gel network can no longer exist, and the modulus is dominated by cage effect (CS60, CS50). The real effective volume fraction increases with Φ_{PSS}, and there is strong long-range electrostatic interaction in PSS glass, which may lead to higher modulus of glass than that of gel.

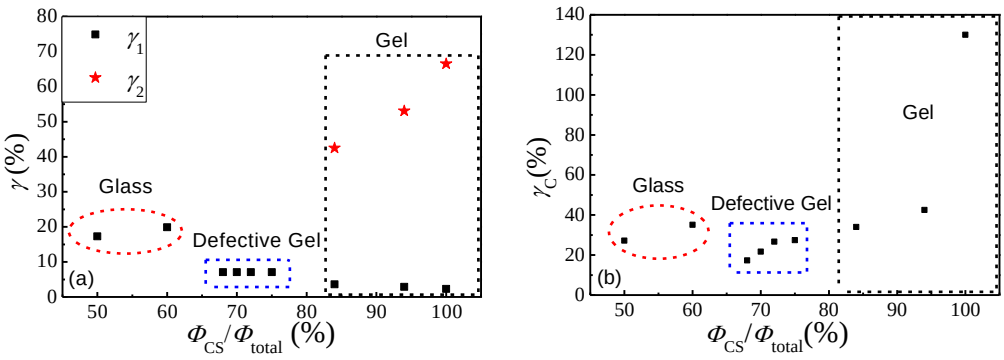

Fig. 9 Yield strains as a function of Φ_{CS}/Φ_{total} acquired from dynamic strain sweeps, Φ_{total} =0.32 is fixed. (a) the first and second yield strain γ_1, γ_2 (b) crossover yield strain γ_C of G' and G''

4.2. Schematic of Defective Gel and Glass

In Fig. 10, the defective gel and glass are schematically illustrated. When Φ_{PSS}/Φ_{total} is low, CS microgels percolate a gel network due to Van der Waals attraction at 35 ℃, while some PSS particles are dispersed in the gel domains and act as defects to weaken the gel, as shown in Fig. 10a. Two possibilities are considered in the kinetic trapping of PSS particles. For case **I**, PSS particle 1 and CS microgels 2 randomly arrange at room temperature. After the temperature increases above the VPTT, an attraction occurs between the microgels, so the microgels tend to stick to each other, forming a gel network. During this process, PSS particle 1 is trapped in the gel region composed of CS microgels 2, which causes CS microgels 2 to share less bonds with their neighbors. In case **II**, CS microgels 4 tend to stick to each other to form a bond, but PSS particles 3 are kinetically stuck between them during the aggregation process, thus weakening the bond. When Φ_{PSS}/Φ_{total} is higher than a threshold, the gel network

can no longer be formed and the biphasic mixture directly jams to generate a glass (Fig. 10b).

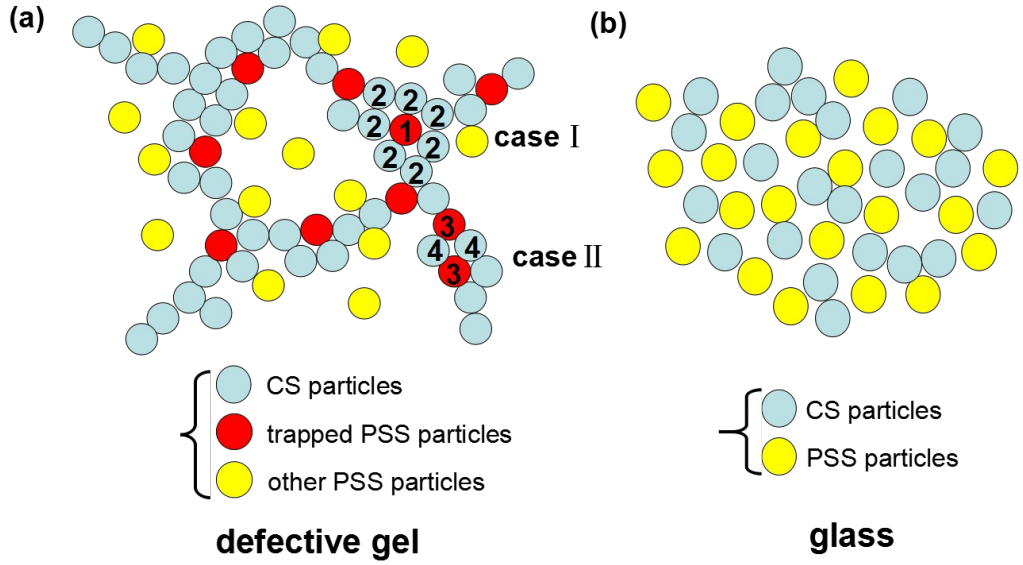

Fig. 10 Schematic illustration of (a) defective gel and (b) glass.

4.3 Construction of State Diagram

Lastly, a hypothetical state diagram for the biphasic mixture is constructed (Fig. 11). In the plot, the relative volume fraction of CS species Φ_{CS}/Φ_{total} *vs* temperature T ($\Phi_{total}=\Phi_{PSS}+\Phi_{CS}=32\%$ is fixed above the LCST) is represented. Above the LCST, when Φ_{CS}/Φ_{total} is higher than 75%, two-step yielding occurs and is defined as the gel region (I). As Φ_{CS}/Φ_{total} decreases below 75%, two-step yielding merges into one-step yielding while the yield strain remains constant at 7%; this particular regime is defined as the defective gel region (II). As Φ_{CS}/Φ_{total} decreases further below a threshold, no percolated network can be formed and the system jams into the glass region (III). Besides, CS microgels are thermo-sensitive and fully swollen at low temperature with repulsive interaction,[38] which causes them to occupy a higher volume fraction. As a result, the gel/defective gel (region I and II) to fluid (region IV)

to repulsive glass (region V) transition will appear as temperature decreases. Therefore, biphasic mixtures exhibit rich state behaviors. Additional work is necessary to explore and understand the mechanisms of the coupling of various transitions.

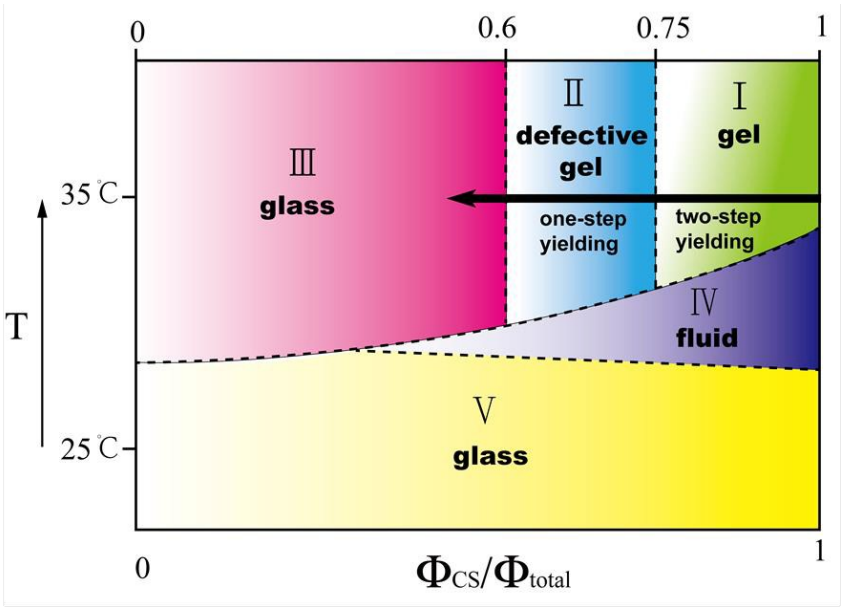

Fig. 11 A hypothetical state diagram of biphasic mixtures drawn in Φ_{CS}/Φ_{total}-T space at fixed $\Phi_{total}=\Phi_{PSS}+\Phi_{CS}=32\%$ above the LCST. The black line with an arrow in the diagram indicates the experimental results in this paper.

5.Conclusions

In summary, a gel-to-defective gel-to-glass transition is studied in a biphasic mixture by varying the relative fraction of CS/PSS at fixed Φ_{total}. From gel to defective gel, two-step yielding merges into one-step, which is an indication of inter-cluster bond breakage coinciding with intra-cluster bond breakage. Some PSS particles are kinetically trapped in the gel and act as defects to weaken the gel strength. With the increase of Φ_{PSS}, the fractal dimension, which reflects the fractal structure of the gel,

gradually changes. When Φ_{PSS} is above a critical value, the system exhibits characteristics of glass, and the modulus is larger than that of gel. Besides, confocal images show that the Φ_{CS}/Φ_{total} dependence of structure evolution is consistent with rheological results. Finally, a hypothetical state diagram is constructed for the biphasic system to illustrate their rich states.

Acknowledgements

The financial support from the National Basic Research Program of China (973 Program, 2012CB821500) and National Natural Scientific Foundation of China (No. 21174152 and No. 21474119) is gratefully acknowledged. Javoris V. Hollingsworth is supported by the National Science Foundation (OISE-1159189). We would like to thank professor Fan Jin in Hefei National Laboratory for Physical Sciences at the Microscale, University of Science & Technology of China for the kindly help on the high resolution confocal microscopy experiment.

Notes and references

1. W. Poon, *Science*, 2004, **304**, 830-831.
2. J. Mewis and N. J. Wagner, *Colloidal Suspension Rheology*, Cambridge University Press, Cambridge, New York, 2012.
3. R. A. L. Jones, *Soft Condensed Matter*, Oxford University Press, Oxford, USA, 2002.
4. R. Mezzenga, P. Schurtenberger, A. Burbidge and M. Michel, *Nat. Mater.*, 2005, **4**, 729-740.

5. C. Gallegos and J. M. Franco, *Curr. Opin. Colloid Interface Sci.*, 1999, **4**, 288-293.

6. T. Cosgrove, *Colloid science: principles, methods and applications*, John Wiley & Sons, Bristol, UK, 2010.

7. P. N. Pusey, *J. Phys.: Condens. Matter*, 2008, **20**, 494202.

8. J. Mattsson, H. M. Wyss, A. Fernandez-Nieves, K. Miyazaki, Z. Hu, D. R. Reichman and D. A. Weitz, *Nature*, 2009, **462**, 83-86.

9. T. Mason and D. Weitz, *Phys. Rev. Lett.*, 1995, **75**, 2770-2773.

10. N. Koumakis, A. Pamvouxoglou, A. S. Poulos and G. Petekidis, *Soft Matter*, 2012, **8**, 4271-4284.

11. K. N. Pham, G. Petekidis, D. Vlassopoulos, S. U. Egelhaaf, P. N. Pusey and W. C. K. Poon, *Europhys. Lett.*, 2006, **75**, 624.

12. T. Sentjabrskaja, E. Babaliari, J. Hendricks, M. Laurati, G. Petekidis and S. U. Egelhaaf, *Soft Matter*, 2013, **9**, 4524-4533.

13. T. Sentjabrskaja, M. Hermes, W. C. K. Poon, C. D. Estrada, R. Castaneda-Priego, S. U. Egelhaaf and M. Laurati, *Soft Matter*, 2014, **10**, 6546-6555.

14. C. Mayer, E. Zaccarelli, E. Stiakakis, C. N. Likos, F. Sciortino, A. Munam, M. Gauthier, N. Hadjichristidis, H. Iatrou, P. Tartaglia, H. Lowen and D. Vlassopoulos, *Nat. Mater.*, 2008, **7**, 780-784.

15. N. Koumakis and G. Petekidis, *Soft Matter*, 2011, **7**, 2456-2470.

16. M. Laurati, S. U. Egelhaaf and G. Petekidis, *J. Rheol.*, 2011, **55**, 673-706.

17. Z. Shao, A. S. Negi and C. O. Osuji, *Soft Matter*, 2013, **9**, 5492-5500.

18. J. P. Segovia-Gutiérrez, C. L. A. Berli and J. de Vicente, *J. Rheol.*, 2012, **56**, 1429-1448.

19. Z. Zhou, J. V. Hollingsworth, S. Hong, H. Cheng and C. C. Han, *Langmuir*, 2014, **30**, 5739-5746.

20. D. C. Viehman and K. S. Schweizer, *J. Chem. Phys.*, 2008, **128**, 084509.

21. D. C. Viehman and K. S. Schweizer, *Phys. Rev. E*, 2008, **78**, 051404.

22. V. Trappe, V. Prasad, L. Cipelletti, P. N. Segre and D. A. Weitz, *Nature*, 2001, **411**, 772-775.

23. J. C. Conrad, S. R. Ferreira, J. Yoshikawa, R. F. Shepherd, B. Y. Ahn and J. A. Lewis, *Curr. Opin. Colloid Interface Sci.*, 2011, **16**, 71-79.

24. A. Mohraz, E. Weeks and J. Lewis, *Phys. Rev. E*, 2008, **77**, 060403.

25. M. Shibayama, T. Tanaka and C. C. Han, *J. Chem. Phys.*, 1992, **97**, 6829-6841.

26. J. E. Smay, G. M. Gratson, R. F. Shepherd, J. Cesarano and J. A. Lewis, *Adv. Mater.*, 2002, **14**, 1279-1283.

27. Q. Li and J. A. Lewis, *Adv. Mater.*, 2003, **15**, 1639-1643.

28. S. K. Rhodes, R. H. Lambeth, J. Gonzales, J. S. Moore and J. A. Lewis, *Langmuir*, 2009, **25**, 6787-6792.

29. P. W. Cox, F. Spyropoulos and I. T. Norton, in *Modern Biopolymer Science*, ed. S. Kasapis, I. T. Norton and J. B. Ubbink, Academic Press, San Diego, 2009, pp. 199-224.

30. N. Dingenouts, C. Norhausen and M. Ballauff, *Macromolecules*, 1998, **31**, 8912-8917.

31. C. Zhao, G. Yuan, D. Jia and C. C. Han, *Soft Matter*, 2012, **8**, 7036-7043.

32. D. Jia, H. Cheng, J. F. Yang and C. C. Han, *Acta Polym. Sin.*, 2015, **5**, 564-570.

33. J. J. Crassous, M. Siebenbürger, M. Ballauff, M. Drechsler, O. Henrich and M. Fuchs, *J. Chem. Phys.*, 2006, **125**, 204906.

34. G. Bryant, S. Martin, A. Budi and W. van Megen, *Langmuir*, 2003, **19**, 616-621.

35. J. J. Crassous, L. Casal-Dujat, M. Medebach, M. Obiols-Rabasa, R. Vincent, F. Reinhold, V. Boyko, I. Willerich, A. Menzel, C. Moitzi, B. Reck and P. Schurtenberger, *Langmuir*, 2013, **29**, 10346-10359.

36. A. G. Marangoni, *Phys. Rev. B*, 2000, **62**, 13951-13955.

37. W. Wolthers, D. van den Ende, V. Breedveld, M. Duits, A. Potanin, R. Wientjes and J. Mellema, *Phys. Rev. E*, 1997, **56**, 5726-5733.

38. G. Romeo, A. Fernandez-Nieves, H. M. Wyss, D. Acierno and D. A. Weitz, *Adv. Mater.*, 2010, **22**, 3441-3445.

39. M. Laurati, G. Petekidis, N. Koumakis, F. Cardinaux, A. B. Schofield, J. M. Brader, M. Fuchs and S. U. Egelhaaf, *J. Chem. Phys.*, 2009, **130**, 134907.

40. A. Ponton, A. Bee, D. Talbot and R. Perzynski, *J. Phys.: Condens. Matter*, 2005, **17**, 821-836.

41. M. Muthukumar, *Macromolecules*, 1989, **22**, 4656-4658.

42. N. K. Reddy, Z. K. Zhang, P. Lettinga, J. Dhont and J. Vermant, American Institute of Chemical Engineers, New York, 2010.

43. K. van der Vaart, Y. Rahmani, R. Zargar, Z. Hu, D. Bonn and P. Schall, *J. Rheol.*, 2013, **57**, 1195-1209.

44. J. Wu, G. Huang and Z. Hu, *Macromolecules*, 2003, **36**, 440-448.

45. H. K. Chan and A. Mohraz, *Phys. Rev. E*, 2012, **85**, 041403.

46. N. Koumakis, J. F. Brady and G. Petekidis, *Phys. Rev. Lett.*, 2013, **110**, 178301.

Table of Contents Entry

Coupling of gelation and glass transition in a biphasic colloidal mixture —from gel-to-defective gel-to-glass

Di Jia,[1,2] Javoris V. Hollingsworth,[1] Zhi Zhou,[1,2] He Cheng[3,4*] and Charles C. Han[1,*]

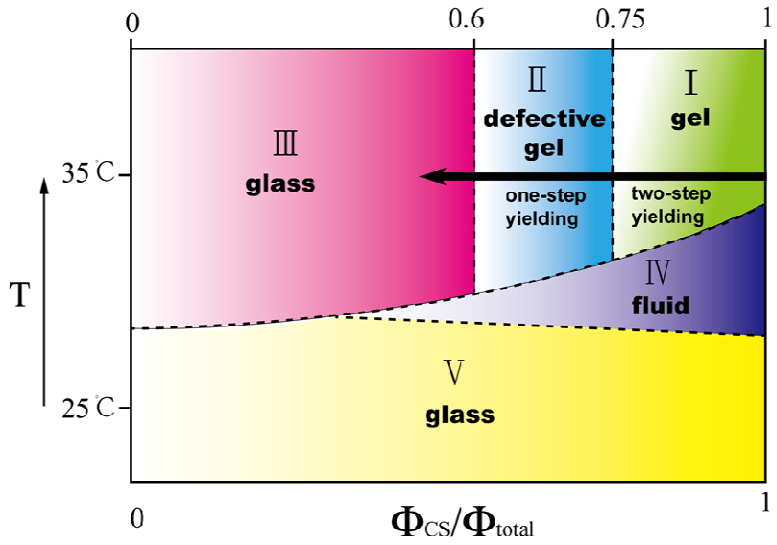

$\Phi_{total}=\Phi_{PSS}+\Phi_{CS}=32\%$ is fixed above the LCST